

Biological response to climate change on a tropical mountain

J. Alan Pounds*†, Michael P. L. Fogden*† & John H. Campbell*

* Golden Toad Laboratory for Conservation, Monteverde Cloud Forest Preserve and Tropical Science Center, Santa Elena, Puntarenas 5655, Box 73, Costa Rica, Central America

† Department of Biology, University of Miami, PO Box 249118, Coral Gables, Florida 33124-0421, USA

Recent warming has caused changes in species distribution and abundance¹⁻³, but the extent of the effects is unclear. Here we investigate whether such changes in highland forests at Monteverde, Costa Rica, are related to the increase in air temperatures that followed a step-like warming of tropical oceans in 1976 (refs 4, 5). Twenty of 50 species of anurans (frogs and toads) in a 30-km² study area, including the locally endemic golden toad (*Bufo perigrinus*), disappeared following synchronous population crashes in 1987 (refs 6-8). Our results indicate that these crashes probably belong to a constellation of demographic changes that have altered communities of birds, reptiles and amphibians in the area and are linked to recent warming. The changes are all associated with patterns of dry-season mist frequency, which is negatively correlated with sea surface temperatures in the equatorial Pacific and has declined dramatically since the mid-1970s. The biological and climatic patterns suggest that atmospheric warming has raised the average altitude at the base of the orographic cloud bank, as predicted by the lifting-cloud-base hypothesis^{9,10}.

This hypothesis builds on evidence that rising sea surface temperatures (SSTs) have altered the climates of tropical mountains. Enhanced evaporation from warm ocean surfaces has generated large amounts of water vapour, and latent heat released as this

moisture condenses has accelerated atmospheric warming⁵. Because vertical thermal profiles have tended towards a moist adiabatic lapse rate, the decline in temperature with increasing elevation has diminished, amplifying the warming in the highlands relative to the lowlands¹¹⁻¹³. Freezing heights have shifted upwards¹¹, and glaciers on high tropical mountains are rapidly melting¹⁴. If temperature-dependent relative humidity surfaces, and thus cloud-formation heights, have likewise shifted upwards¹⁰, organisms may be affected in various ways. Monteverde's stratus-stratocumulus bank, which forms as the trade winds meet the Caribbean slope of the Cordillera de Tilarán, flow upwards and cool adiabatically, influences several key ecological processes. A lifting cloud base should alter regional hydrology by reducing critical dry-season inputs of mist (low-intensity windblown precipitation) and cloud water (non-precipitating droplets deposited onto vegetation)^{15,16}.

To examine climate trends, we have analysed patterns of precipitation, stream flow, air temperatures and SSTs. The rainfall and air-temperature data (collected by J.H.C.) are from leeward cloud forest (1,540 m; ~1 km west of the Monteverde Cloud Forest Preserve headquarters and ~3 km west of the continental divide). The weather station lies on the western boundary of our 30-ha study plot for anoline lizards, which overlaps a 40-ha plot for birds. Both plots lie within the 30-km² anuran study area. The stream-flow data (from the Costa Rican Electrical Institute) are for the Río Cañas at Líbano (300 m; ~23 km northwest of Monteverde). The SST data (from NOAA) are for the Niño-3 region of the equatorial Pacific (~850 km SW; 150° W-90° W, 5° N-5° S).

Using daily rain-gauge records from the dry season (January-April), we develop a mist-frequency index. These data underestimate windblown inputs¹⁶ but contain signatures of mist events (as well as rare convective showers and wind-driven rains during cold fronts). Because 'dry days' (ones without measurable precipitation) represent intervals with little or no mist, their pattern conveys information about the incidence and temporal distribution of mist events. The frequency of dry days is inversely related to mist frequency, so we use the former as a negative index of the latter.

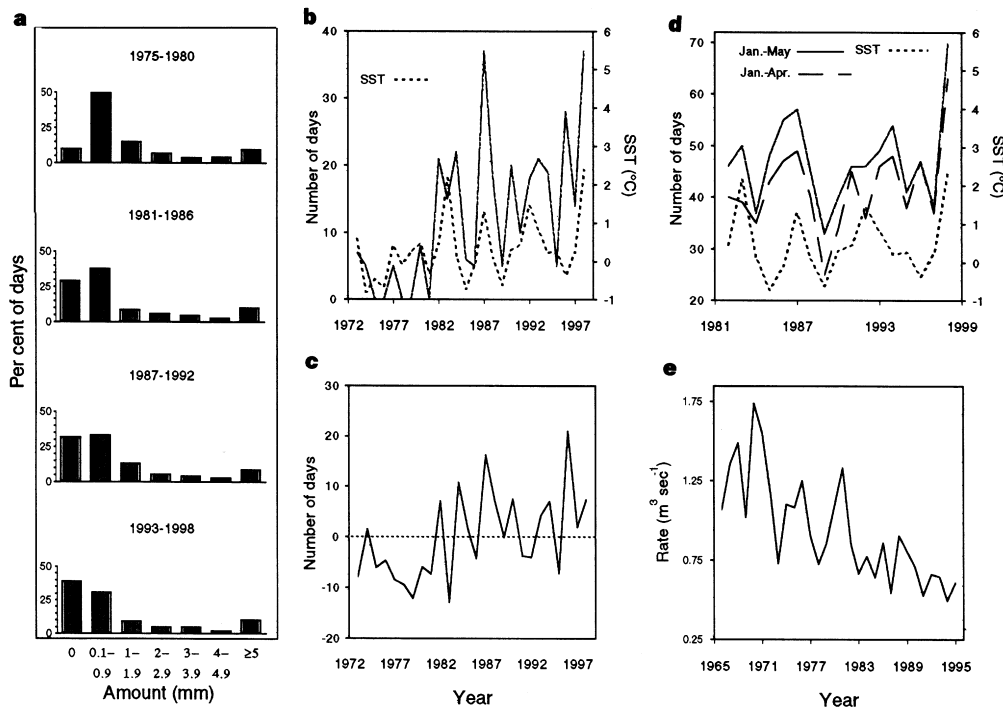


Figure 1 Trends and fluctuations in dry-season precipitation and stream flow. **a**, Frequency distributions of daily rainfall by 6-yr periods. **b**, SSTs (mean anomalies) and dry days in runs ≥ 5 . In the stepwise multiple regression, both SST and year explained significant amounts of variation in the number of dry days

(*t*-tests for partial coefficients, $P < 0.01$; for the full model, $F_{2,23} = 14.4$, $P < 0.001$; $r^2 = 0.56$). **c**, The drying trend, as illustrated by the residuals from step 1 of this regression (that is, the effect of year partialled on SST). **d**, Recent ENSOs and total dry days. **e**, Annual minimum stream flow (minimum daily average).

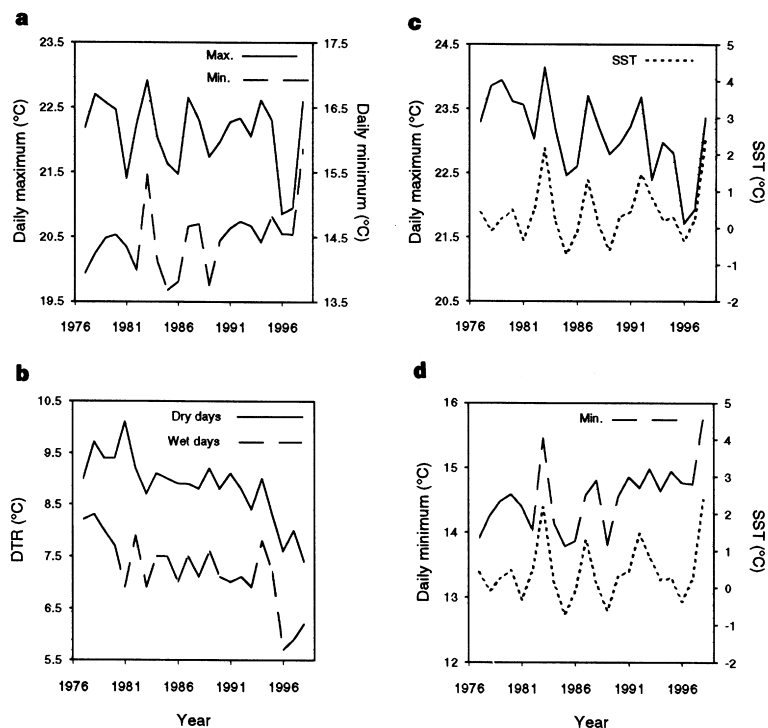


Figure 2 Trends and fluctuations in dry-season air temperatures. **a**, Daily minima and maxima (means). Test for trends: for the mean minimum, $r_s = 0.51, P < 0.016, N = 22$; for the mean maximum, $r_s = -0.19, P > 0.4$; for the mean DTR, $r_s = -0.64, P < 0.0002$ **b**, Diurnal temperature range (DTR) for wet days and

dry days (ones with and without measurable precipitation). Tests for trends: for wet days, $r_s = -0.64, P < 0.002$; for dry days, $r_s = -0.78, P < 0.0001$; **c**, SSTs (mean anomalies) and daily maxima on dry days. **d**, SSTs and daily minima on wet days.

As predicted by the lifting-cloud-base hypothesis, this index indicates a decline in mist frequency. Annual, seasonal and monthly rainfall totals show no trends over 1973–98. Day-to-day variability (the coefficient of variation of daily totals) likewise shows no trend for the wet season (May–October) or the transitional season (November–December). It exhibits a positive trend, however, for the dry season, mainly because dry days have increased in frequency (Fig. 1a). They have also increasingly coalesced into runs (Fig. 1b; up to 16 days). Although these dry periods are associated with warm episodes of the El Niño/Southern Oscillation (ENSO), the drying trend remains significant after ENSO-scale fluctuations are taken into account (Fig. 1b, c). Warm episodes, together with this underlying trend, produced the four largest recorded peaks in total dry days (in 1983, 1987, 1994 and 1998; Fig. 1d). Annual minimum stream flow, correlated with mist frequency, likewise indicates an ENSO-related signal superimposed on a drying trend (Fig. 1e).

Trends in dry-season air temperatures also accord with the lifting-cloud-base hypothesis. Because the daily minimum has increased relative to the daily maximum, the diurnal temperature range (DTR, the difference between the two) has declined (Fig. 2a). The negative trend implies increasing cloudiness, which lowers daytime temperatures by blocking solar radiation and raises night-time temperatures by reducing radiative heat losses^{17,18}. The coefficient of variation of DTR shows no trend, suggesting that day-to-day variability of cloudiness has not changed. Dry days exhibit larger DTRs than ‘wet days’ (ones with measurable precipitation), but the negative trend in DTR applies to both (Fig. 2b). The former result agrees with our observation that dry days often occur under clear skies. The trend for dry days implies that their numbers have increased by the addition of dry, cloudy days, as would be expected if a lifting cloud base has increased the fraction of non-precipitating clouds. This trend is not due entirely to changes in daily minima: daily maxima have declined, suggesting afternoon cloudiness on the added dry days (Fig. 2c). The nocturnal warming trend is strongest for wet days (Fig. 2d). Both daily maxima and minima are correlated

with SSTs (Fig. 2c, d).

The trends in DTR run counter to other proposed explanations for the decline in mist frequency: (1) the frequency of cloud-bank formation may have decreased; or (2) the average position of the cloud bank’s leeward (western) edge may have receded eastward, beyond our weather station, if lee warming and drying have changed. These hypotheses, which envisage an increased frequency of clear skies over this station, predict a decrease in cloudiness or an increase in its day-to-day variability.

Changes in bird abundance at 1,540 m support the prediction that species should respond to climate change according to their distributions along climatic gradients¹⁹. Examining data for 1979–98 (collected by M.P.L.F.), we calculate trends in abundance (inferred from observation frequency) for two categories of species: (1) ‘lower montane’—the breeding fauna of cloud forest ($\geq 1,470$ m) in the baseline years (1979–81); and (2) ‘premontane’—cloud-forest-intolerant species, which bred only in premontane areas ($< 1,470$ m) during 1979–81. In the 1,540-m plot, the former shows no consistent pattern, whereas the latter chiefly exhibits increases (Fig. 3a).

Accordingly, the number of lower-montane species present in this plot has remained comparatively stable, whereas that of premontane species has increased (Fig. 3b). The increase has not been monotonic, because species that have extended their distributions upslope have often shifted back down. Net colonization (the number moving up minus the number moving down) is positive in some years and negative in others. The average rate, estimated as the slope of the linear regression, is 19 species per decade (excluding wide-ranging raptors and swifts, often recorded as flyovers). Colonizing species represent a broad taxonomic and ecological range and have come from premontane areas of both the Caribbean and Pacific slopes.

Fifteen colonizing species have established breeding populations in the 1,540-m plot, which have generally increased in density. For instance, golden-crowned warblers (*Basileuterus culicivorus*) first

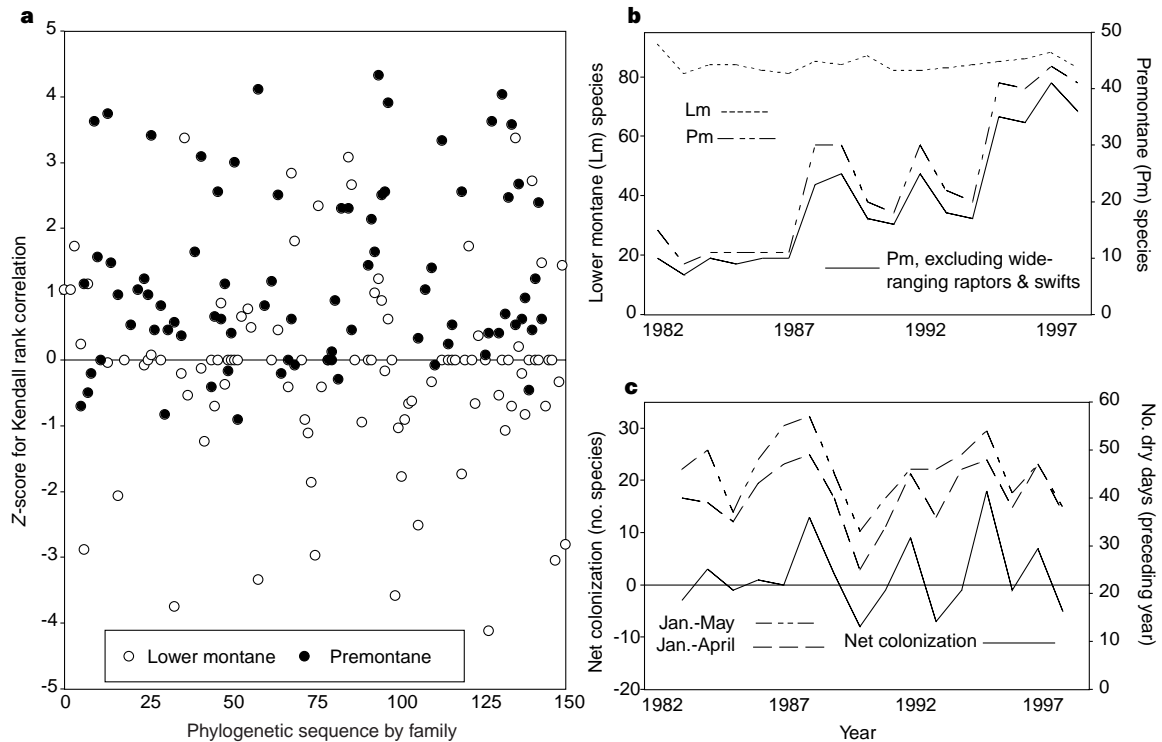


Figure 3 Changes in the bird community of the 1,540-m plot. **a**, Trends in abundance of individual species in relation to breeding distribution (lower montane versus premontane) in the baseline years. Values are normal approximations (Z) for Kendall's τ corrected for ties. Positive scores indicate increases, negative ones decreases. **b**, Trends in numbers of species present.

For lower-montane species, $\tau = 0.18$, $P > 0.34$, $N = 17$; for premontane species, $\tau = 0.67$, $P < 0.005$. **c**, Climate and upslope colonization. In the multiple regression, number of dry days in the preceding year's dry season accounted for 53% of the variation in net colonization.

nested there in 1994 (3 pairs) but increased to 20 pairs by 1998. Lesser greenlets (*Hylophilus decurtatus*) first nested there in 1988 (2 pairs) but had increased to 12 pairs by 1998. Although some recent arrivals remain at low density, their presence nevertheless represents significant change. Keel-billed toucans (*Ramphastos sulfuratus*; 2 pairs in 1998) previously bred only in lowlands and foothills²⁰; since 1995 they have nested alongside resplendent quetzals (*Pharomachrus moccino*), which symbolize Middle American cloud forests.

Habitat alteration has contributed to changes in distribution and abundance but cannot easily explain the patterns at 1,540 m. The mosaic of forest and clearings outside the Monteverde Preserve dates to the 1940s and early 1950s; no major deforestation has occurred in recent decades. This mosaic, which lies mostly in premontane areas, should favour upslope colonization by open-country birds, which increase in abundance relative to forest birds where there are clearings. The patterns at 1,540 m, however, apply to both.

Moreover, these patterns are strongly related to variation in mist frequency. Of various climatic variables tested by multiple regression, total dry days in the preceding year's dry season is by far the best predictor of upslope movements (Fig. 3c). A model based on 1982–96 patterns⁹ correctly predicted the sign and magnitude of net colonization in 1997 and 1998. Although a weak response to the 1982–83 El Niño is evident, the first major influx of colonists followed the 1986–87 warm episode.

Anoline lizard populations, which are sensitive to rainfall variability²¹, have declined in association with the same mist-frequency patterns. In the 1,540-m plot, two highland species endemic to Costa Rica and western Panama (the cloud forest anole, *Norops tropidolepis*, and the montane anole, *N. alatae*) began to decline in the late 1980s and had disappeared by 1996 (Fig. 4a). In contrast to these species, the gray lichen anole (*N. intermedius*), which is most abundant in warmer, drier areas further down the Pacific slope^{8,22}, shows no trend at 1,540 m (ref. 8). For each

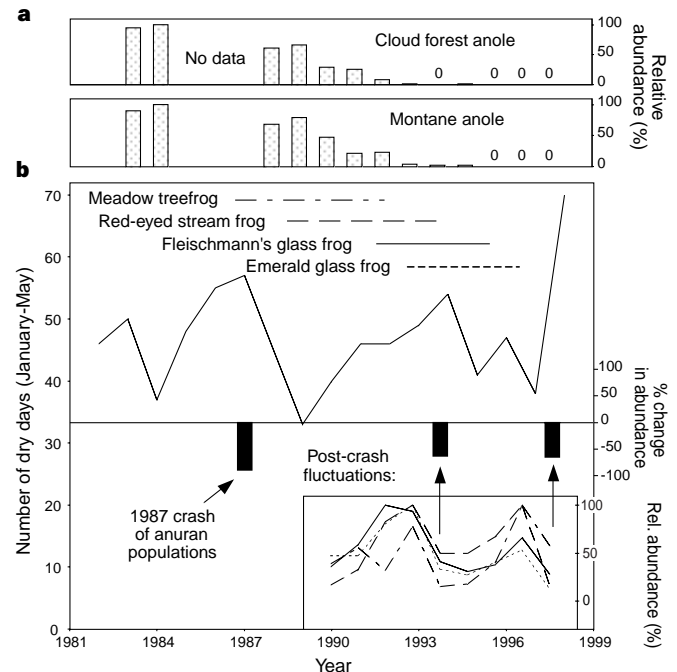


Figure 4 Declines in populations of anoline lizards and anurans. **a**, Anoles. For correlations of abundance with number of dry days in the preceding dry season, $\tau \leq -0.55$, $P < 0.016$, $N = 11$ yrs. **b**, Anurans. The random probability (P) that a population downturn would correspond to one of the 3 largest peaks in total dry days equals the proportion of years exhibiting these peaks. Thus, for 1984–98, $P = 3 \text{ peaks} \div 15 \text{ yr} = 0.2$ (a conservatively high estimate because the climatic extremes are the largest during 1973–98). Substituting 0.2 in a binomial distribution, we calculate the maximum probability that all three demographic events would, by chance alone, correspond to these extremes to be 0.008.

declining species, wet-season abundance is negatively correlated with total dry days in the preceding dry season but shows no correlation with other climatic variables tested.

The anuran declines, although more episodic than the anole declines, are likewise associated with mist-frequency patterns. To follow changes after the 1987 crashes, J.A.P. and co-workers have monitored selected populations since 1990⁷. Wet-season abundances of four aquatic-breeding species, which have fluctuated far below pre-crash levels, underwent synchronous downturns in 1994 and 1998 (Fig. 4b). Thus, three demographic events—in 1987, 1994, and 1998—correspond to the three largest peaks in total dry days. The probability that all three events would, by chance alone, correspond to these climatic extremes is ≤ 0.008 (Fig. 4b). Because anuran populations ordinarily fluctuate with climate, the 1987 crashes conceivably were due to an external event (such as the arrival of a pathogen) that coincided by chance with the 1986–87 warm episode. Similarities between demographic events suggest, however, that the climatic patterns are more than incidental to the declines. For example, red-eyed stream frogs (*Hyla uranochroa*) at several sites underwent extinctions in both 1987 and 1998, the most extreme years climatically. (The frogs had recolonized in the intervening years.) Populations of terrestrial-breeding rain frogs (*Eleutherodactylus diastema*) likewise crashed over large areas in 1987 and 1998 (J.A.P., unpublished results).

The changes in populations of birds, lizards and anurans are concordant yet diverse. All are associated statistically with the same climatic patterns and occurred simultaneously, implying a broad response to regional climate change which crossed an important threshold in the late 1980s. Although one study concluded that anuran declines in Australia are probably not climate-related²³, the analyses relied on monthly weather data. The reduction in mist frequency reported here, which agrees with large-scale climate trends^{5,11–13} and simulations of greenhouse warming¹⁰, is evident only in the daily records. The diversity of demographic changes related to this reduction suggests that climate has orchestrated them by means of several biotic mechanisms (although climate may also interact with other physical factors⁶). Evidence that dry weather in 1983 increased the vulnerability of harlequin frogs (*Atelopus varius*) to lethal parasites along one stream^{24–26} inspired the “climate-linked epidemic hypothesis”²⁶. As the habitat dried and the frogs gathered near waterfalls, their probability of being attacked by parasitic flies increased sharply: forty dead or dying frogs were observed. Because climate affects host–parasite relationships²⁷ and amphibians^{28,29} in various ways, it may have set the stage for similar mortality events, including those ascribed to chytrid fungus outbreaks³⁰. If so, the recent, widespread amphibian extinctions in seemingly undisturbed highland forests may attest to how profound and unpredictable the outcome can be when climate change alters ecological interactions. □

Methods

Precipitation and stream flow. We examine rainfall trends for 1973–98 ($N = 26$; Spearman rank correlations, r_s ; $\alpha = 0.05$; 2-tailed). Time series are short considering potential interdecadal variability but cover the critical period of oceanic warming. Analyses of dry-season frequency distributions (Fig. 1a) focus on January–April, but we tally dry days (Fig. 1b–d) for January–May. The dry season sometimes extends beyond April, depending on when convective rains begin. The number of days comprising dry periods has increased, regardless of the definition of minimum period length (≥ 1 , ≥ 2 , ..., ≥ 10 days). Whereas total dry days exhibits lag-1 autocorrelation, the number in runs ≥ 5 does not, and thus meets independence assumptions for F statistics. We regress the latter variable on SST and year in a stepwise analysis. SSTs are anomalies (deviations from the running mean) averaged for January–May. We screened SSTs from the different Niño regions (and the Southern Oscillation Index): Niño-3 values exhibit the strongest correlations with precipitation variables. To examine stream-flow patterns, we use Fourier analysis. Deforestation may have contributed to the downward trend by altering runoff patterns. The clearings,

however, date to the 1960s or earlier, whereas minimum flow has continued to decline in the 1980s and 1990s.

Air temperatures. We examine trends for 1977–98 ($N = 22$; Fig. 2). Because we use means for January–May to match our tallies of dry days, the inferred increase in cloudiness may involve convective cumulus and cumulonimbus, as well as advective status and stratocumulus. (Convection increases in frequency over January–May as the trade winds subside; it typically becomes the dominant pattern in early-to-middle May.) The negative trend in DTR, however, applies to data subsets that progressively reduce the influence of convection (Jan–Apr, Jan–Mar, Jan–Feb, and January), suggesting effects of advective clouds.

Birds. The 1979–81 survey of the Monteverde region included 13.5 months of sampling ($>2,000$ h). To calculate individual species trends (Fig. 3a), we examine observation frequencies (proportions of 6-day periods in which a species was present) over 1982–98 ($N = 17$). Number of periods sampled was ≥ 10 per primary breeding season (March–July) and similar for the remaining months (total, 499; $>15,000$ h). Sampling included daily listening to the dawn chorus from key points, plus surveys of a 2-km circuit (2 per period) within the 40-ha plot (25 ha of primary forest, 13 ha of secondary forest, 2 ha meadows). We examine observation frequencies weighted to equalize contributions of breeding and non-breeding seasons. Analyses of unweighted data, however, give virtually identical results, as do analyses for the breeding season only. To estimate changes in breeding density of recent arrivals, we compare observations in the year of first breeding to singing-male counts in 1998. Independent variables in the multiple regression analysis (Fig. 3c) include annual and seasonal mean daily rainfall, number of dry days (Jan–Apr, Jan–May, runs ≥ 3 , runs ≥ 5 , and longest run), and mean temperature (daily maximum, daily minimum, and DTR). We also include each variable with its effect lagged by 1 year.

Anoline lizards and anurans. We calculate the relative abundance of anoles (per cent of the maximum yearly average for 1983–98) from counts of adults during the wet season (≥ 10 2-h surveys per yr)⁸. Correlations with climatic variables are based on data through 1996, when both species had disappeared from the study area ($N = 11$). Variables tested are listed above (see Birds). Pounds *et al.*⁷ have described study sites and methods used to monitor meadow treefrogs (*Hyla pseudopuma*), red-eyed stream frogs (*Hyla uranochroa*), Fleischmann’s glass frogs (*Hyalinobatrachium fleischmanni*), and emerald glass frogs (*Centrolenella prosoblepon*). For each species in each wet season, we average abundances of the different populations and calculate relative abundance (per cent of the maximum yearly average for 1990–98). Per cent change for 1987 is a conservative estimate derived from baseline observations and 1990 data for the same four species.

Received 24 November 1998; accepted 25 February 1999.

1. Parmesan, C. Climate and species’ range. *Nature* **382**, 765–766 (1996).
2. Veit, R. R., McGowan, J. A., Ainley, D. G., Wahls, T. R. & Pyle, P. Apex marine predator declines 90% in association with changing oceanic climate. *Global Change Biol.* **3**, 23–28 (1997).
3. McGowan, J. A., Cayán, D. R. & Dorman, L. M. Climate–ocean variability and ecosystem response in the northeast Pacific. *Science* **281**, 210–217 (1998).
4. Trenberth, K. E. & Hurrell, J. W. Decadal atmosphere–ocean variations in the Pacific. *Clim. Dyn.* **9**, 303–319 (1994).
5. Graham, N. E. Simulation of recent global temperature trends. *Science* **267**, 666–671 (1995).
6. Pounds, J. A. & Crump, M. L. Amphibian declines and climate disturbance: the case of the golden toad and the harlequin frog. *Cons. Biol.* **8**, 72–85 (1994).
7. Pounds, J. A., Fogden, M. P. L., Savage, J. M. & Gorman, G. C. Tests of null models for amphibian declines on a tropical mountain. *Cons. Biol.* **11**, 1307–1322 (1997).
8. Pounds, J. A. in *Monteverde: Ecology and Conservation of a Tropical Cloud Forest* (eds Nadkarni, N. M. & Wheelwright, N. T.) (Oxford University Press, New York, in press).
9. Pounds, J. A., Fogden, M. P. L. & Campbell, J. H. in *Meeting Report, Bird Life International/WWF Workshop on the Impacts of Climate Change on Flora and Fauna* (ed. Briggs, B.) (Royal Society for Protection of Birds, Bedfordshire, UK, 1997).
10. Still, C. J., Foster, P. N. & Schneider, S. H. Simulating the effects of climate change on tropical montane cloud forests. *Nature* **398**, 608–610 (1999).
11. Diaz, H. F. & Graham, N. E. Recent changes in tropical freezing heights and the role of sea-surface temperature. *Nature* **383**, 152–155 (1996).
12. Beniston, M., Diaz, H. F. & Bradley, R. S. Climatic change at high elevation sites: an overview. *Clim. Change* **36**, 233–251 (1997).
13. Diaz, H. F. & Bradley, R. S. Temperature variations during the last century at high elevation sites. *Clim. Change* **36**, 253–279 (1997).
14. Thompson, L. G. *et al.* Late glacial stage and holocene tropical ice core records from Huascarán, Peru. *Science* **269**, 46–50 (1995).
15. Cavalier, J., Solis, D. & Jaramillo, M. A. Fog interception in montane forests across the Central Cordillera of Panamá. *J. Trop. Ecol.* **12**, 357–369 (1996).
16. Clark, K. L., Nadkarni, N. M., Schaefer, D. & Gholz, H. Atmospheric deposition and net retention of ions by the canopy in a tropical montane forest, Monteverde, Costa Rica. *J. Trop. Ecol.* **14**, 27–45 (1998).
17. Karl, T. R. *et al.* A new perspective on recent global warming: asymmetric trends of daily maximum and minimum temperatures. *Bull. Am. Meteorol. Soc.* **74**, 1007–1023 (1993).

18. Gómez, I. E. & Fernandez, W. Variación interanual de la temperatura en Costa Rica. *Top. Meteor. Oceanogr.* **3**, 27–44 (1996).
19. Karr, J. R. & Freemark, K. E. Habitat selection and environmental gradients: dynamics in the 'stable' tropics. *Ecology* **64**, 1481–1494 (1983).
20. Fogden, M. P. L. *An Annotated Checklist of the Birds of Monteverde and Peñas Blancas* (Green Mountain, Monteverde, Costa Rica, 1993).
21. Andrews, R. M. Population stability of a tropical lizard. *Ecology* **72**, 1204–1217 (1991).
22. Pounds, J. A. Ecomorphology, locomotion, and microhabitat structure: patterns in a tropical mainland *Anolis* community. *Ecol. Monogr.* **58**, 299–320 (1988).
23. Laurance, W. F. Catastrophic declines of Australian rainforest frogs: is unusual weather responsible? *Biol. Cons.* **77**, 203–212 (1996).
24. Crump, M. L. & Pounds, J. A. Lethal parasitism of an aposematic anuran (*Atelopus varius*) by *Notochaeta bufonivora* (Diptera: Sarcophagidae). *J. Parasitol.* **71**, 588–591 (1985).
25. Pounds, J. A. & Crump, M. L. Harlequin frogs along a tropical montane stream: aggregation and the risk of predation by frog-eating flies. *Biotropica* **19**, 306–309 (1987).
26. Crump, M. L. & Pounds, J. A. Temporal variation in the dispersion of a tropical anuran. *Copeia* **1989**, 209–211 (1989).
27. Dobson, A. & Carper, R. in *Global Warming and Biological Diversity* (eds Peters, R. L. & Lovejoy, T. E.) 201–217 (Yale Univ. Press, New Haven, Connecticut, 1992).
28. Beebe, T. J. C. Amphibian breeding and climate. *Nature* **374**, 219–220 (1995).
29. Stewart, M. M. Climate driven population fluctuations in rain forest frogs. *J. Herpetology* **29**, 437–446 (1995).
30. Berger, L. et al. Chytridiomycosis causes amphibian mortality associated with population declines in the rain forests of Australia and Central America. *Proc. Natl Acad. Sci.* **95**, 9031–9036 (1998).

Acknowledgements. We thank C. J. Still, P. N. Foster and S. H. Schneider for sharing their GCM simulations and for their comments on the manuscript; we also thank M. Brenes, R. W. Carlson, P. M. Fogden, G. R. Graves, J. F. Jackson, F. J. Joyce, K. L. Masters, J. M. Savage and N. T. Wheelwright for comments that improved the final version. J.A.P. acknowledges partial support from the MacArthur Foundation, Stanford University's Center for Conservation Biology, the Brookfield Zoo, the University of Miami, the US NSF, the Jessie Smith Noyes Foundation, the Organization for Tropical Studies, the Tropical Science Center and the University of Florida.

Correspondence and requests for materials should be addressed to J.A.P. (e-mail: goldtoad@sol.racs.a.co.cr).

Humans use internal models to estimate gravity and linear acceleration

Daniel M. Merfeld*†, Lionel Zupan* & Robert J. Peterka

Neurological Sciences Institute, Oregon Health Sciences University, 1120 NW 20th Avenue, Portland, Oregon 97209, USA

* These authors contributed equally to this work.

Because sensory systems often provide ambiguous information, neural processes must exist to resolve these ambiguities. It is likely that similar neural processes are used by different sensory systems. For example, many tasks require neural processing to distinguish linear acceleration from gravity¹, but Einstein's equivalence principle states that all linear accelerometers must measure both linear acceleration and gravity. Here we investigate whether the brain uses internal models, defined as neural systems that mimic physical principles, to help estimate linear acceleration and gravity^{2–4}. Internal models may be used in motor control^{5–7}, sensorimotor integration^{8–10} and sensory processing^{11–14}, but direct experimental evidence for such models is limited. To determine how humans process ambiguous gravity and linear acceleration cues, subjects were tilted after being rotated at a constant velocity about an Earth-vertical axis. We show that the eye movements evoked by this post-rotational tilt include a response component that compensates for the estimated linear acceleration even when no actual linear acceleration occurs. These measured responses are consistent with our internal model predictions that the nervous system can develop a non-zero estimate of linear acceleration even when no true linear acceleration is present.

When present, inter-aural linear acceleration has been shown^{15–17} to elicit a compensatory horizontal eye movement, the vestibulo-ocular reflex (VOR). A similar horizontal VOR might occur if the nervous system uses an internal model to mimic the external physical relationship¹ (Fig. 1, $F = G - A$) between gravity (G),

linear acceleration (A), and specific gravito-inertial force (GIF, F). Specifically, we propose that an internal (neural) model of this physical relationship exists (Fig. 2, $\hat{F} = \hat{G} - \hat{A}$), with the difference between the internal estimates of gravity (\hat{G}) and linear acceleration (\hat{A}) equalling the estimated GIF (\hat{F}). A non-zero estimate of linear acceleration will arise whenever there is a mismatch between the internal estimate of gravity and the physiological measurement of GIF, and a compensatory horizontal VOR will be evoked whenever the estimate of linear acceleration includes a non-zero, inter-aural component (\hat{A}_y , Fig. 2c).

To investigate these predictions, eight subjects (including four experienced psychophysical observers) were seated upright and rotated at a constant angular velocity of 200° s^{-1} about an Earth-vertical axis for 150 s. The rotating subjects were then rapidly decelerated (100° s^{-2}) to a stop. Immediately after stopping, subjects were tilted by 90° about an axis through the centre of the head (at ear level) in 1.5 s, to one of eight evenly spaced orientations: nose-up (NU), nose-down (ND), right-down (RD), left-down (LD), and each of the four orientations midway between these principal orientations (NU-RD, NU-LD, ND-RD, ND-LD). The trial order was randomized and secret; the direction of rotation and the direction of tilt were counter-balanced. Binocular eye movements were recorded in the dark throughout motion and for 150 s following deceleration with bitebar-stabilized video cameras. The video system was calibrated using 29 fixation targets. Video data were analysed off-line to give horizontal eye position, which was digitally differentiated to give horizontal eye velocity. Fast phases were removed using a computer algorithm, with some manual editing by experienced personnel, leaving the slow phase velocity.

Constant velocity rotation followed by tilt ('post-rotational tilt') was chosen to elicit a mismatch between estimated gravity and true gravity (Fig. 2). Deceleration to a stop following constant velocity rotation induces a strong cue from the semicircular canals which indicates rotation, due to the peripheral dynamics of the semicircular canals¹⁸. This cue falsely signals angular velocity in the direction opposite to the preceding rotation, even though the subject is at rest. At the same time, graviceptors (for example, vestibular otolith organs) measure a constant, unchanging, gravito-inertial force, resulting in a contradictory sensory situation. The illusory sensations induced by this and similar paradigms are "confusing, unpleasant, and difficult to describe"¹⁹. Rotational cues are known to influence the perceived orientation of gravity²⁰, often leading to illusory tilt²¹. Therefore, we suggest that the yaw rotational cue following post-rotational tilt leads to illusory tilt and that the direction of the illusory tilt matches the direction of tilt that would occur if the rotational cue were accurate.

To measure illusory tilt, the four subjects who were experienced psychophysical observers verbally answered standard questions regarding their subjective tilt more than 2 min after tilting. (A

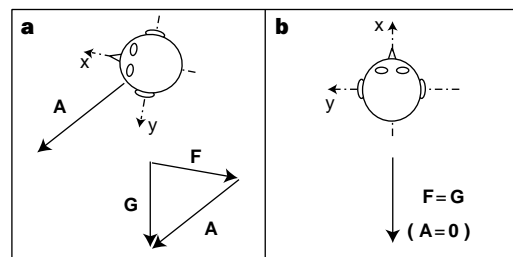


Figure 1 During acceleration on Earth, gravity (G) minus linear acceleration (A) yields specific gravito-inertial force (GIF, F). Different combinations of gravity and linear acceleration can yield the same measured GIF. **a**, GIF equals gravity minus linear acceleration ($F = G - A$ or $F + A = G$). **b**, GIF equals gravity alone. Since the measurement of GIF relative to the head is identical for these two situations, additional information is required for the nervous system to determine how much of the measured GIF is due to gravity and how much is due to linear acceleration.

† Present address: Vestibular Physiology Laboratory, Massachusetts Eye and Ear Infirmary, 243 Charles Street, Boston, MA 02114, USA.